

Ionization reactions of ion complexes in mesoscopic water clusters

Styliani Consta

FOM Institute of Atomic and Molecular Physics (AMOLF), Kruislaan 407, 1098 SJ Amsterdam, The Netherlands

Raymond Kapral

Chemical Physics Theory Group, Department of Chemistry, University of Toronto, Toronto, Ontario M5S 3H6, Canada

(Received 18 May 1999; accepted 11 August 1999)

The free energy and dynamics of the dissociation reactions of the $[\text{Na}^+(\text{Cl}^-)_2]$ ion complex in mesoscopic water clusters are examined. The free energy surface shows the existence of stable single and double solvent-separated complex species formed from ionization of the stable double-contact ion complex. The reaction occurs on the cluster surface for mesoscale clusters composed of tens of water molecules. Passage between stable species is an activated process but barrier crossing has a large diffusive component so that dynamical corrections to transition state theory are large. The structure of the decay of the time-dependent rate constant reflects the diffusive character of the recrossing dynamics so that a plateau is not established on a 10 ps time scale in contrast to ionization dynamics in bulk fluids. © 1999 American Institute of Physics. [S0021-9606(99)51941-7]

I. INTRODUCTION

Reactions in mesoscopic liquid clusters differ from their bulk counterparts because the interplay between interior and surface forces can give rise to selective solvation and modify reaction dynamics. Consequently, experimental investigations of cluster structure and dynamics have received increasing attention.¹⁻³ In this article we investigate the mechanisms and dynamics of the interconversion reactions of an ion complex with an excess negative ion in a mesoscopic water cluster. Studies of the mechanisms and dynamics of ionization reactions in water clusters have fundamental as well as practical interest;^{4,5} for example, complexes of ions participate in a number of atmospheric reactions which take place on or in water clusters. In bulk liquids it is well known that the solvent is responsible for the existence of chemical species such as solvent-separated ion pairs (SSIP) and influences the rate at which transitions take place between contact ion pairs (CIP) and SSIP or ionization to free ions.^{6,7}

The $\text{CIP} \rightleftharpoons \text{SSIP}$ reaction for $\text{Na}^+ - \text{Cl}^-$ has been extensively investigated in bulk water^{8,9} as have the properties of $\text{Na}^+ - \text{Na}^+$ and $\text{Cl}^- - \text{Cl}^-$ ion pairs.¹⁰ There have also been studies of the structure and reaction dynamics of ion pairs in bulk model aprotic polar solvents.¹¹

Ion pair solvation has been investigated in clusters. Studies of small aqueous clusters containing $\text{K}^+ - \text{Cl}^-$ ion pairs¹² have shown that the presence of a few water molecules can lead to a substantial reduction in the interionic attraction and that the stabilities of the CIP and SSIP species depend on the cluster size. For large interionic separations, the solvent forces play a cohesive role preventing the ions from escaping the clusters. Similar results were observed for $\text{Na}^+ - \text{Na}^+$ and $\text{Cl}^- - \text{Cl}^-$ ion pairs in water clusters¹² and in the dissociation reaction of HCl in the aprotic acetonitrile and dimethylsulfoxide solvents where quantum effects are important.¹³

Theoretical models for ion solvation in clusters have been proposed^{14,15} and computer simulation results may be used to assess the validity of the assumptions made in the development of such analytical models. The general question of the mechanisms of ion solvation underlies the solvation dynamics in these more complex ion pair systems and considerable effort has been devoted to solvent reorganization in clusters containing a single ion.¹⁶

We focus on the mechanisms and rates of certain steps of the ionization reactions of $[\text{Na}^+(\text{Cl}^-)_2]$ in water clusters. For these more complex systems it is reasonable to assume a scheme analogous to the $\text{CIP} \rightleftharpoons \text{SSIP}$ interconversion process for ion pairs; however, new solvent-separated species may exist since one or both of Cl^- ions may reside in a solvent-separated position relative to the Na^+ ion.

The structure of the article is as follows: in Sec. II the model system and simulation method are described. Section III contains a study of the free energy of the system as a function of the coordinates of the ion complex. The free energy surface is used to identify stable chemical species and suggest reaction pathways between them. The dynamics of the ionization reactions is the topic of Sec. IV. Here estimates of the rate constants are given and other details of the dynamics are studied. The conclusions of this study are made in Sec. V.

II. SYSTEM AND SIMULATION METHODS

The system consists of an ion complex $[\text{Na}^+(\text{Cl}^-)_2]$ embedded in a 70-molecule water cluster. The ion-ion potential is of the Huggins-Mayer type and is expressed as the sum of a Coulomb potential and a short-range repulsive potential which accounts for excluded volume effects:

$$V_{ij}(r) = A_{ij} \exp(-r/\rho_{ij}) + \frac{z_i z_j e^2}{r}. \quad (1)$$

Here z_i is the charge on ion i , $+1$ and -1 for the Na^+ and Cl^- ions, respectively. The ions interact with the water molecule sites via Coulomb and Lennard-Jones (LJ) potentials.

In the simulations the extended simple point charge model (SPC/E)¹⁷ is used. The hydrogen–oxygen distance is 1.0 \AA . The bond angle interaction is harmonic and is given by $V = (1/2)k(\theta - \theta_0)^2$ where $k = 383 \text{ kJ mol}^{-1} \text{ rad}^{-2}$ and $\theta_0 = 109.47$.¹⁸ The interaction between two water molecules a and b is given by:

$$V_{ab} = 4\epsilon_{\text{OO}} \left[\left(\frac{\sigma_{\text{OO}}}{r_{\text{OO}}^{ab}} \right)^{12} - \left(\frac{\sigma_{\text{OO}}}{r_{\text{OO}}^{ab}} \right)^6 \right] + \frac{1}{4\pi\epsilon_0} \sum_{i=1}^3 \sum_{j=1}^3 \frac{z_i^a z_j^b}{r_{ij}^{ab}}. \quad (2)$$

The charges on the water sites are $z_{\text{H}^+} = 0.4238e$ and $z_{\text{O}^-} = -0.8476e$ and the LJ parameters are $\sigma_{\text{OO}} = 3.166 \text{ \AA}$ and $\epsilon_{\text{OO}} = 0.6502 \text{ kJ mol}^{-1}$. The SPC/E model was chosen for the simulations since it yields good interfacial¹⁸ and solvation properties.⁹ There are Coulomb interactions between the ions and the sites of water. Between the oxygen sites and the ions LJ interactions are also present with parameters, $\epsilon_{\text{NaO}} = 0.54392 \text{ kJ mol}^{-1}$, $\sigma_{\text{NaO}} = 2.350 \text{ \AA}$, $\epsilon_{\text{ClO}} = 0.4184 \text{ kJ mol}^{-1}$, $\sigma_{\text{ClO}} = 4.400 \text{ \AA}$.

The molecular dynamics simulations were performed using constant energy molecular dynamics after a thermalization period during which constant temperature dynamics was used. The classical equations of motion were integrated using the Verlet algorithm¹⁹ with a time step of 2 fs. The constraints used to fix the intramolecular bond lengths were treated using the SHAKE algorithm.²⁰ Nosé–Hoover dynamics²¹ was used during the 80–100 ps thermalization period. The temperature of the system was $T = 240 \text{ K}$ and in the course of the simulations evaporation was rarely observed.

Clusters containing 70 water molecules and an $[\text{Na}^+(\text{Cl}^-)_2]$ ion complex were studied. Such clusters are large enough to support two water solvation shells around the ion complex. Henceforth, when we wish to distinguish the two Cl^- ions in the complex, we denote them by $\text{Cl}_{(1)}^-$ and $\text{Cl}_{(2)}^-$ and the corresponding $\text{NaCl}_{(1)}$ and $\text{NaCl}_{(2)}$ interion separations are denoted by r_1 and r_2 . Convenient coordinates to describe the ion complex configurations are these two interion separations and the ClNaCl angle θ . Free energy surfaces projected onto the (r_1, r_2) plane were computed using the constrained-reaction-coordinate dynamics (CRCD) ensemble.²²

III. ION COMPLEX STRUCTURE AND IONIZATION MECHANISMS

A. Free energy of $[\text{Na}^+(\text{Cl}^-)_2]$

The free energy as a function of the coordinates of the ion complex plays a central role in studies of solvation since minima in the free energy surface may be used to define chemical species and its topography suggests possible reaction pathways. Below we shall compute and analyze the free energy projected onto the (r_1, r_2) coordinates of the complex. The free energy, $W(r_1, r_2)$, may be defined in terms of the probability density $P(r_1, r_2)$ for finding the coordinates of the complex at (r_1, r_2) : $W(r_1, r_2) = -kT \ln P(r_1, r_2)$. A

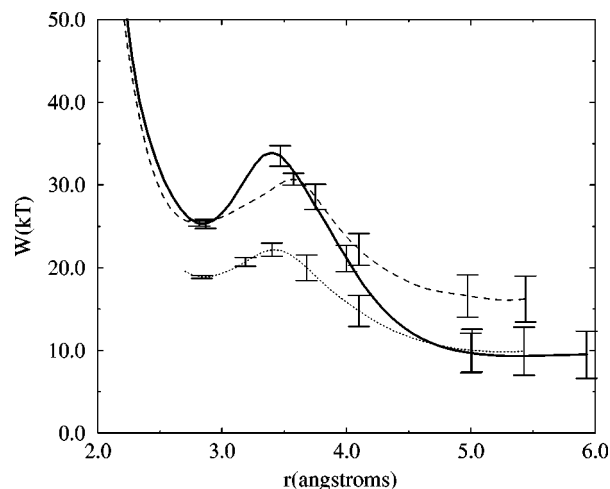


FIG. 1. Sections through the three-dimensional free energy surface for $[\text{Na}^+(\text{Cl}^-)_2]$. The solid line represents the section along the diagonal, the dashed line and the dotted line correspond to $r_1 = 2.9 \text{ \AA}$, and $r_1 = 4.7 \text{ \AA}$, respectively. The error bars are \pm one standard deviation.

crude estimate of $W(r_1, r_2)$ may be obtained from histograms of r_1 and r_2 in a long, unconstrained molecular dynamics trajectory. The results of such simulations show prominent free energy minima at $(r_1, r_2) \approx (2.9, 2.9)$, $(r_1, r_2) \approx (2.9, 4.7)$, $(r_1, r_2) \approx (4.7, 2.9)$, and $(r_1, r_2) \approx (4.7, 4.7)$.

Quantitative free energy results were determined from constrained molecular dynamics simulations.²² The mean force was computed for various values of r_2 along lines $r_1 = \text{const}$ passing through the minima. A coordinate transformation was made to express the Cartesian coordinates of $\text{Cl}_{(1)}$ and $\text{Cl}_{(2)}$ in spherical polar coordinates with center at Na. In this coordinate system the mean force is

$$F(r_2; r_1) = \frac{\langle (-\hat{\mathbf{r}}_2 \cdot \partial V / \partial \mathbf{r}_2 + \beta^{-1} 2/r_2) D^{-1/2} \rangle}{\langle D^{-1/2} \rangle}, \quad (3)$$

where β is the inverse of $k_B T$, V is the total potential of the system which includes solvent-ion and interionic interactions, and

$$D = \frac{1}{\mu} \left(1 - \frac{\mu^2}{m_{\text{Na}}} \cos^2 \theta \right), \quad (4)$$

with m_{Na} the mass of Na, μ the reduced mass of Na and $\text{Cl}_{(1)}$, and θ the ClNaCl angle. The free energy may be determined by integration of the mean force,

$$W(r_2; r_1) = - \int_{\infty}^{r_2} F(r'_2; r_1) dr'_2 + C, \quad (5)$$

where C provides a reference point for the free energy.

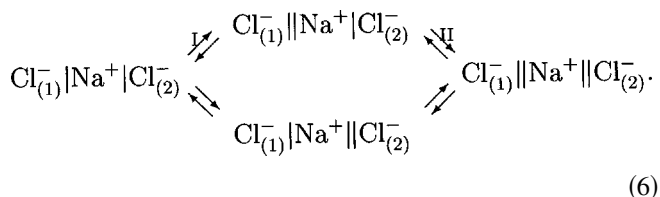
The mean force (3) for $[\text{Na}^+(\text{Cl}^-)_2]$ was computed from 0.8 ns constant energy trajectories following a 100 ps thermalization period and the potentials of mean force,²³ determined from integration (5), are shown in Fig. 1 for sections along $r_1 = 2.85, 4.7 \text{ \AA}$, along with the section for $r_1 = r_2$. In these graphs the common points of the sections along $r_1 = 2.9 \text{ \AA}$ and $r_1 = 4.7 \text{ \AA}$ with the diagonal were matched. The locations of the extrema and the energy differences are shown in Table I. The free energy sections suggest that a

TABLE I. Location of the extrema and depths of the wells with respect to the barrier top for sections of the three-dimensional free energy surface for $[\text{Na}^+(\text{Cl}^-)_2]$ in SPC/E water clusters.

$[\text{Na}^+(\text{Cl}^-)_2]$			Barrier heights (kT)	
$(r_1(\text{\AA}), r_2(\text{\AA}))$			ΔE_1	ΔE_{-1}
First minimum	Maximum	Second minimum		
(2.9,2.9)	(2.9,3.5)	(2.9,4.75)	5.4	15.7
(4.75,2.9)	(4.75,3.4)	(4.75,4.75)	3.3	12.3
(2.9,2.9)	(3.4,3.4)	(4.75,4.75)	8.5	24.6

local maximum exists at $(r_1, r_2) = (3.5 \text{ \AA}, 3.5 \text{ \AA})$ along the path with $r_1 = r_2$. Henceforth, we denote the ion complex species in the vicinity of $(r_1, r_2) \approx (2.85, 2.85)$ as CIP = $[\text{Cl}|\text{Na}|\text{Cl}]^-$; the species near $(r_1, r_2) \approx (2.85, 4.7)$ or $(r_1, r_2) \approx (4.7, 2.85)$ as SSIP(1) = $[\text{Cl}|\text{Na}|\text{Cl}]^-$ or $[\text{Cl}|\text{Na}|\text{Cl}]^-$, and that near $(r_1, r_2) \approx (4.7, 4.7)$ as SSIP(2) = $[\text{Cl}|\text{Na}|\text{Cl}]^-$.

A schematic representation of the two-dimensional free energy surface deduced from the free energy sections is shown in Fig. 2 where the reaction channels along which computations are performed are indicated. Figure 3 shows the reactions that take place along the channels. From the topography of this surface one may postulate that these solvation species undergo the following interconversion reactions denoted by steps I and II:



The minimum free energy path appears to lie along the $r_1 = 2.85 \text{ \AA}$ section and is assigned to step I of the reaction scheme; the section along $r_2 = 4.7 \text{ \AA}$ is assigned to step II of the reaction scheme. Since the maximum energy state of the diagonal path III corresponds to a global maximum in the reversible work surface this path is unlikely to be taken.

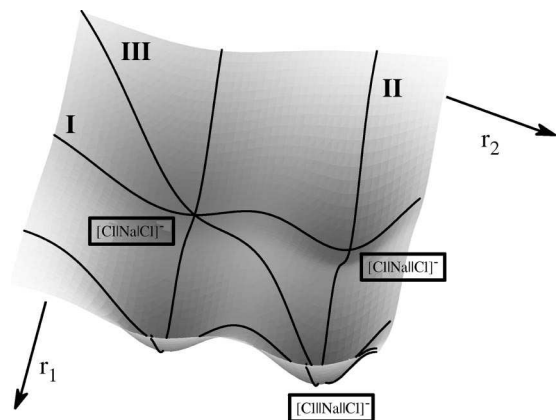


FIG. 2. Schematic representation of the three-dimensional free energy surface of $[\text{Na}^+(\text{Cl}^-)_2]$ in the presence of 70 water molecules.

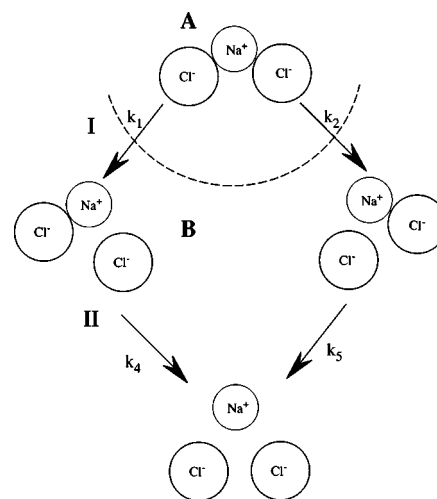


FIG. 3. Schematic graph of the reaction channels and partitioning of the configuration space into A and B species. The section of a circle indicated by a dashed line represents the dividing surface. By symmetry $k_1 = k_2$ and $k_4 = k_5$.

B. Reaction mechanisms

The description of the configurational changes in the structure of the ion complex and the solvent reorganization that accompanies the transitions among the various solvation species constitutes the mechanism of the reaction. We shall show that the reaction mechanism involves the ion complex and solvent reorganizations depicted in Figs. 5 and 6.

First we examine the probability distributions of θ , the ClNaCl angle, which were not considered in the free energy studies. Probability density profiles $P(\theta)$ for complex configurations at the stable and transition states are shown in Fig. 4. For reaction step (I), θ of the reactant state is strongly peaked near 110° while in the transition state this angle is

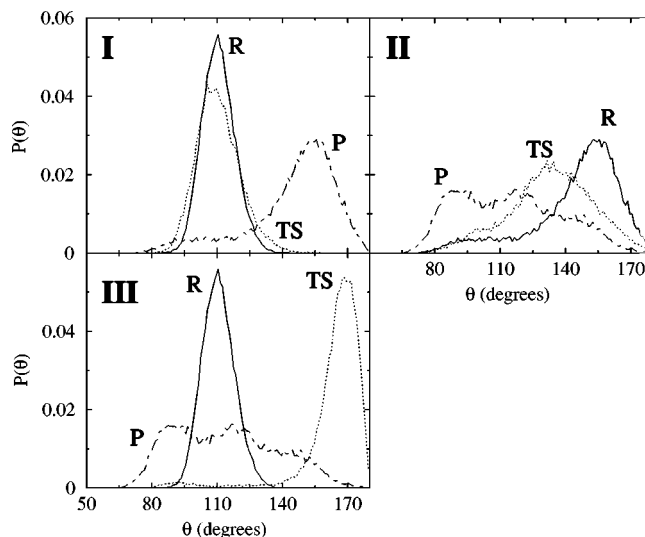


FIG. 4. Probability density of the ClNaCl angle, $P(\theta)$: (a) for reaction step (I), (b) for reaction step (II), (c) for reaction step (III). The solid, dotted, and dashed-dotted lines correspond to the reactant (R), transition state (TS), and product (P) states, respectively. The configurations used to construct these densities were collected every 0.1 ps in the course of a 1.0 ns constrained dynamics trajectory. The bin size is 1 deg.

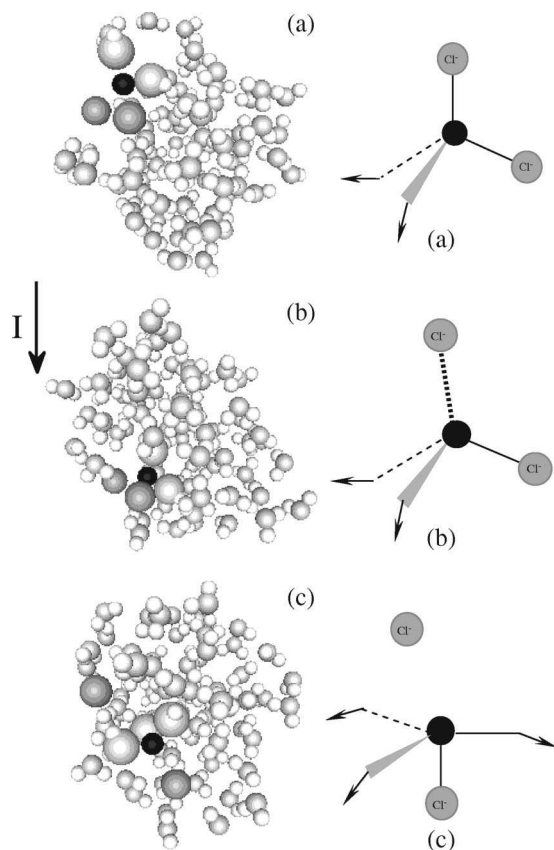


FIG. 5. First column: snapshots of the reactant, product, and transition states for reaction channel (I). The sizes of the oxygen sites closest to Na⁺ have been enlarged relative to the oxygen sites in the remaining water molecules in the cluster. The large dark gray colored spheres and the small black colored sphere represent the two Cl⁻ ions and Na⁺, respectively. Second column: schematic representation of the reaction. The water dipoles in the first solvation shell of Na⁺ are represented by arrows.

near 105° [Fig. 4(I)]. The transition state resembles the reactant state and there are no pronounced changes in the local structure of the complex. In the product state $P(\theta)$ is peaked near 155° and has a long tail that extends up to 80°. This suggests that isomerisation “reactions” may take place where the two Cl⁻ ions are found in almost *cis* or *trans* conformations. In step (II) of the reaction [Fig. 4(II)], the reactant is the product of step (I). The transition state $P(\theta)$ distribution is different from the reactant state. The ClNaCl angle is compressed with a peak at $\approx 130^\circ$. In the product state $P(\theta)$ shows an almost uniform distribution in the range of 65° to 155°. Since the two Cl⁻ ions are not tightly bound to the Na⁺ there is freedom in their motion. For comparison, in Fig. 4(III) we show $P(\theta)$ for configurations along the diagonal $r_1 = r_2$. There is no transition state along this path since a maximum on the free energy surface separates reactants from products.

The second step in examining the mechanism of the reaction is to characterize the reacting species in more detail. Although the detailed picture of the mechanism depends on the exact nature of the interactions, one can extract qualitative information on the role of the solvent in the reaction from the simple water models used in this study. The mechanism of the reaction is shown schematically in Figs. 5 and 6

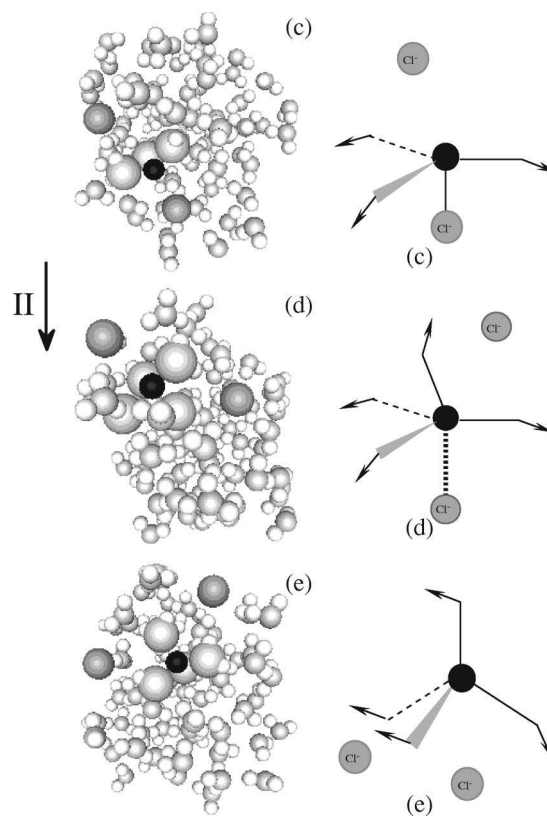


FIG. 6. Same as Fig. 5 but for reaction channel (II).

along with snapshots of the actual cluster configurations taken from the simulations. The arrows on the schematic drawings represent the dipole moments of water and their orientations are obtained from the statistics of the molecular dynamics trajectories. In the transition state, the detachment of particles is indicated by dotted lines, while strong “bonds” between Na⁺ and particles in the first solvation shell are shown by solid lines. In Fig. 5(a) a snapshot of a typical configuration where the complex is in the double-contact form, $(r_1, r_2) \approx (2.9, 2.9)$, is shown. The radial distribution functions show that the first solvation shell of Na⁺ is composed of two water molecules. Examination of the ONaO and ClNaO angles suggests that the two chlorides and the two water molecules of the first solvation shell of Na⁺ form a tetrahedron with small deviations from the 109° tetrahedral angle. The dipoles of the water molecules in the first solvation shell of Na⁺ form a 15° angle with the NaO axis. Figure 5(b) corresponds to the transition state of reaction channel I. In the transition state one of the NaCl bonds is extended. As shown in Fig. 4(I) for the transition state, the distribution of the ClNaCl angle is slightly wider than in the reactant state. While the chloride that is more tightly bound to Na⁺ continues to form an angle of approximately 109° with the oxygens of the first solvation shells, the chloride that is farther from Na⁺ has an ONaCl angle of 97°. The transition state resembles the reactant state; however, the coordination number of Na⁺ is slightly larger than 2. The constrained dynamics trajectories show that a third water molecule rarely visits the first solvation shell of Na⁺. In the single solvent separated form, Fig. 5(c), the coordination

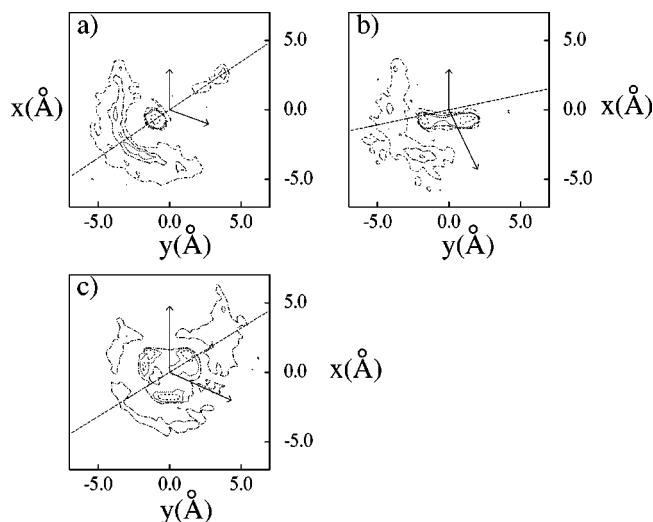


FIG. 7. Probability density of the projection of the oxygen sites on the plane defined by \mathbf{r}_1 and \mathbf{r}_2 . The dashed line shows the bisector of the average ClNaCl angle. (a) $(r_1, r_2) = (2.9 \text{ \AA}, 2.9 \text{ \AA})$ with contour lines at 0.0058, 0.008, 0.01, 0.03; (b) $(r_1, r_2) = (2.9 \text{ \AA}, 4.75 \text{ \AA})$ with contour lines at 0.0058, 0.008, 0.01, 0.02; (c) $(r_1, r_2) = (4.75 \text{ \AA}, 4.75 \text{ \AA})$ with contours at 0.0055, 0.008, 0.0135.

number of Na^+ is 3 and one of the Cl^- ions has detached from the first solvation shell. The structure of the complex is almost bipyramidal in some of the conformations. Conformations which are not bipyramidal also appear since the chloride ion that is farther from Na^+ is more flexible and often attains conformations where it is almost in the same plane with the three water molecules of the first solvation shell.

In path II, the reactant state is the product of path I. In the transition state [Fig. 6(d)] the coordination number of Na^+ is slightly less than 4. Statistics of constrained dynamics trajectories show that a fourth water molecule resides in the first solvation shell of Na^+ for most of the time. The structure of the first coordination shell of Na^+ is close to tetrahedral. In the product state [Fig. 6(e)] four water molecules are found in the first solvation shell of Na^+ , and form an almost perfect tetrahedron.

The picture that emerges from the description of the solvent in the vicinity of the complex in combination with the behavior of the complex is that the ionization reactions occur by concerted motions of the water solvent molecules and ions in the complex. Since the reaction occurs in a finite size system questions concerning the distinct features of the cluster environment enter the mechanism, for example, how accurately the free surface can be used to predict the course of the reaction and how the average cluster structure changes in the course of the reaction. We now examine the behavior of the solvent when the ion complex resides in one of its stable forms. Figure 7 shows the probability density of the projections²⁴ of the positions of the oxygen atoms in the plane defined by \mathbf{r}_1 and \mathbf{r}_2 . The coordinate system is defined by the unit vector $\hat{\mathbf{r}}_1$ and the unit vector perpendicular to it. The arrow heads show the average positions of $\text{Cl}_{(1)}^-$ and $\text{Cl}_{(2)}^-$ with Na^+ at the origin of the axes.

In Fig. 7(a) the average structure of the solvent is shown

while the complex is in the double-contact configuration. The complex lies on the surface of the cluster. The Na^+ resides in the bulk of the cluster and it is strongly solvated compared to the two Cl^- ions. The strong peak at $(x, y) = (-1.0, -1.0)$ is due to the two water molecules of the first solvation shell of Na^+ . One more solvation shell is shown in the figure that suggests a strong ordering of the water molecules. A strong water-molecule peak also appears at $(x, y) = (2.5, 4.0)$. This structure arises from solvent that is found in two sites of the $(\mathbf{r}_1, \mathbf{r}_2)$ plane; these sites are connected by strings of water molecules that cross the $(\mathbf{r}_1, \mathbf{r}_2)$ plane. For this cluster size there is a third shell of surface water molecules for which no contours are shown. The orientation of the molecules on the surface, induced by the presence of the complex, is affected by the existence of the free surface, the diffusive nature of the interface and the faster diffusive motion of the molecules on the surface. In Fig. 7(b) the average structure of the solvent is shown when the complex is in the single solvent-separated configuration. Two intense peaks appear at $(x, y) = (-0.5, 1.5)$, $(-0.5, -2.0)$ which correspond to the three water molecules of the first solvation shell of Na^+ . The effect of the asymmetry of the complex is also clearly reflected in the second solvation shell where the solvent shows a strong peak at $(-3.0, -2.0)$ closer to the longer Na-Cl distance. In Fig. 7(c) the structure of the solvent in the double solvent-separated configuration is shown. The three peaks at $(x, y) = (1.5, 1.5)$, $(-1.5, 0.0)$, $(1.0, -2.0)$ correspond to the four water molecules of the first solvation shell of Na^+ . The intense peaks of the first solvation shell of Na^+ are quite broad since the water molecules of the first solvation shell exchange with molecules of the surroundings. The two Cl^- lie on the surface while the Na^+ tends to be found inside the cluster. The broad solvent structure between the two arrows in the second solvation shell of Na^+ arises from the bulk of the cluster.

Simulations were also performed with a polarizable model of water,²⁵ with parameters taken from Ref. 26 The structure of the solvent is very similar to that of the SPC/E model although the Na^+ is slightly better solvated. Graphs analogous to Fig. 7 are shown in Fig. 8. The qualitative features of the mechanism that are independent of the model are the fact that the reaction proceeds on the surface of the cluster with strong reorganization of the solvent structure. As both the polarization and SPC/E model suggest, in the double and single CIP configurations of the complex, the Na^+ lies within the bulk of the cluster. In the double solvent-separated solvent configurations, the Cl^- ion tends towards the bulk of the cluster, and the Na^+ ion is more strongly solvated. In the course of the reaction the two Cl^- are almost free of water molecules. The region of the cluster in which the reaction occurs will have implications for the mechanism since the coordination number of the reacting species on the surface may be different from that in the bulk, and the motions of the solvent particles on the surface will affect the dynamics of the reaction in a way that differs from that in the bulk phase.

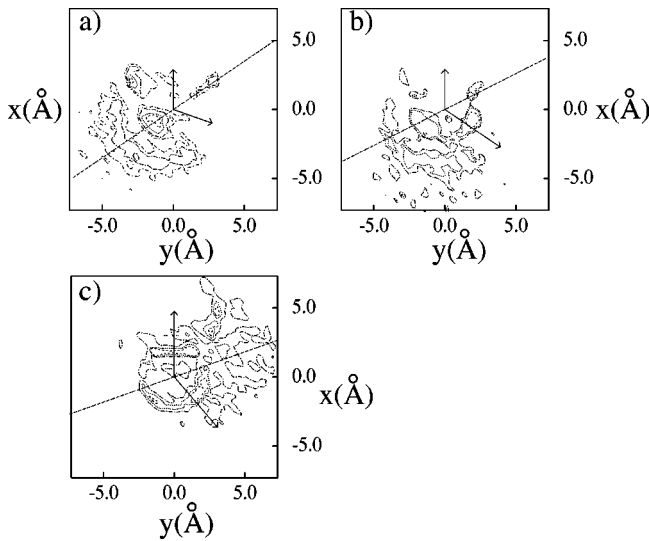


FIG. 8. Same as Fig. 7 but for the polarizable model for water. (a) Contour lines at 0.0058, 0.008, 0.01, 0.013, (b) contour lines at 0.0068, 0.008, 0.011, (c) contour lines at 0.0059, 0.008, 0.010.

IV. DYNAMICS OF $[\text{Na}^+(\text{Cl}^-)_2]$ IONIZATION REACTIONS

A complete investigation of the microscopic dynamics of the ionization reactions in Eq. (6) requires a phase space or configuration space specification of all species involved in the mechanism. Rather than studying all details of this mechanism we focus on the rate at which the $\text{CIP}=\text{A} = [\text{Cl}|\text{Na}|\text{Cl}]^-$ transforms to either of the SSIP(1) forms $[\text{Cl}|\text{Na}||\text{Cl}]^-$ or $[\text{Cl}||\text{Na}|\text{Cl}]^-$. A reaction coordinate that is appropriate for this transformation is

$$\xi(r_1, r_2) = (r_1^2 + r_2^2)^{1/2}, \quad (7)$$

and the configuration space dividing surface $\xi = \xi^\ddagger$ is shown schematically in Fig. 3. Letting B refer to all species for which $\xi(r_1, r_2) > \xi^\ddagger$, we may write the ionization reaction $\text{A} \rightleftharpoons \text{B}$ and use the standard formula,²⁷

$$k_f = \frac{\langle \dot{\xi} \delta(\xi - \xi^\ddagger) \theta(\xi(t) - \xi^\ddagger) \rangle}{\langle \theta(\xi^\ddagger - \xi(t)) \rangle} = k_f^{\text{TST}} \kappa, \quad (8)$$

to compute the forward rate constant. As is usual in such computations, the rate constant may be written as the product of the transition state rate constant k_f^{TST} , which requires a knowledge of the free energy along ξ , and the transmission coefficient κ which accounts for dynamical effects.

The free energy profile for this reaction coordinate was computed using the CRCD ensemble.²² The new set of generalized coordinates consists of the Cartesian coordinates of the water molecule atoms and the sodium ion, the spherical polar coordinates of Cl^- with origin at the sodium ion, and the spherical polar coordinates of a vector with magnitude equal to ξ . The mean force at constrained values of the reaction coordinate was computed from the formula:

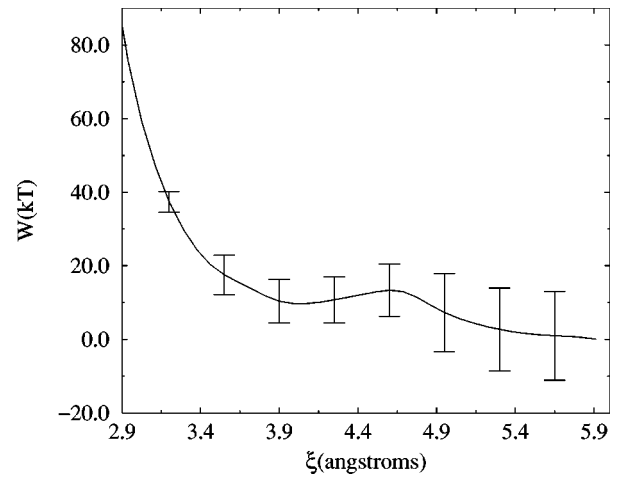


FIG. 9. Free energy along $\xi = (r_1^2 + r_2^2)^{1/2}$.

$$F(\xi) = \langle D^{-1/2} \rangle^{-1} \left\langle \left(-\frac{\xi}{r_2} \frac{\partial V}{\partial \mathbf{r}_2} \cdot \mathbf{r}_2 + \beta^{-1} \frac{-2\xi^2 + r_1^2}{\xi(-\xi^2 + r_1^2)} \right) D^{-1/2} \right\rangle, \quad (9)$$

where

$$D = \xi^{-2} (r_1^2/m_{\text{Cl}(1)} + r_2^2/m_{\text{Cl}(2)} + (\mathbf{r}_1 + \mathbf{r}_2)^2/m_{\text{Na}}). \quad (10)$$

The free energy profile shown in Fig. 9 was obtained from integration of the mean force. The first minimum is located at 4.0 Å and the barrier top is at 4.6 Å. The energy difference between the first minimum and the barrier top is 3.7 kT.

The transition state value ξ^\ddagger was chosen to lie at the barrier top of the free energy as a function of ξ and $\xi^\ddagger(r_1, r_2)$ passes through the transition states for reaction path I. It is instructive to examine the probability distribution of r_1 and r_2 when ξ is constrained at the barrier top. The probability distribution $P(\phi)$ of the angle $\phi = \arctg(r_1/r_2)$, shown in Fig. 10(a), is symmetric with respect to the 45-degree line in accord with the symmetry of the reaction mechanism and exhibits two peaks. In Fig. 10(b) the corresponding free energy given as $W(\phi) = -kT \ln P(\phi)$ is shown. Configurations of the complex with $r_1 = r_2$ occur with low probability while the maxima are found in the vicinities of the path I transition states. Consequently, specific reaction channels exist in (r_1, r_2) space corresponding to $\xi = \xi^\ddagger$.

Figure 10(c) shows the probability distribution of the ClNaCl angle. The angular distribution is similar to that of the transition state for path I. One can also see that there is a small probability of finding angles with values close to 180 deg which suggests that bipyramidal configurations of the complex with the chloride ions at *trans* positions are attained rarely. The bipyramidal configurations lie on trajectories leading to $[\text{Cl}|\text{Na}|\text{Cl}]^-$ or $[\text{Cl}|\text{Na}||\text{Cl}]^-$ since three water molecules are already found in the first hydration shell of Na^+ and this transition state resembles the product state rather than the reactant state.

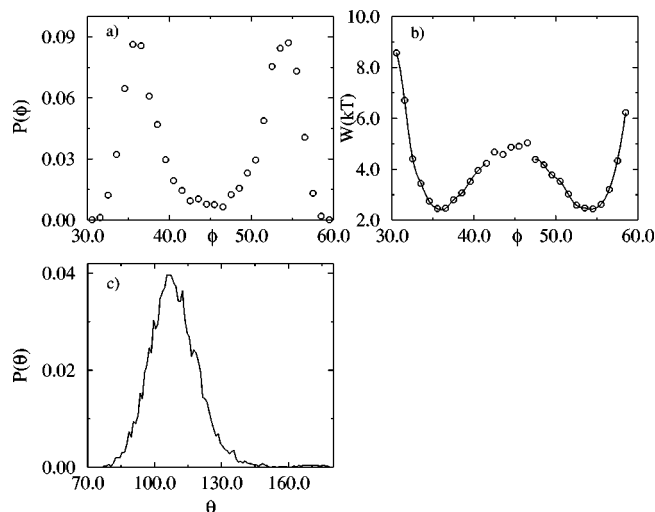


FIG. 10. (a) Probability density of the angle $\phi = \arctg(r_1/r_2)$. (b) Free energy, W with respect to ϕ . The solid line is the cubic spline interpolation through the open circles. The points at the barrier top were not interpolated because the statistics is poorer than at the minima. (c) Probability density of the ClNaCl angle, $P(\theta)$.

A. Rate constant

The rate of the reaction was computed in the following way: statistically independent configurations were selected every 5 ps from a constant temperature simulation where the reaction coordinate was constrained at ξ^\ddagger . Initial velocities were assigned to particles of these configurations according to the generalization of Boltzmann sampling for rigid molecules.²⁸ The constraint on the reaction coordinate was released and the trajectories were evolved forward in time for 5 ps using constant energy molecular dynamics. In the constrained ensemble the transmission coefficient is computed from:

$$\kappa(t) = \frac{\langle D^{-1/2} \dot{\xi} \theta(\xi(t) - \xi^\ddagger) \rangle_c}{\langle D^{-1/2} \dot{\xi} \theta(\dot{\xi}) \rangle_c}, \quad (11)$$

where $\langle \dots \rangle_c$ denotes an average over the constrained ensemble. The transmission coefficient is estimated from the plateau value that may exist after some transient time. A plateau exists provided that the relaxation time for the reaction is much longer than the relaxation time of other processes in the system. The transition state theory result is given by

$$k_f^{\text{TST}} = (2\pi\beta)^{-1/2} \langle D^{-1/2} \rangle_c P(\xi^\ddagger), \quad (12)$$

where $P(\xi^\ddagger) = \delta(\xi - \xi^\ddagger) / \langle \theta(\xi^\ddagger - \xi(t)) \rangle$ is the probability of being at the barrier top, normalized by the reactant density.

Statistical results were obtained from the dynamics of 10 000 trajectories starting at $\xi = \xi^\ddagger$. The transition state theory estimate for the forward rate is 0.28 ps^{-1} (1/3.6 ps). The time-dependent transmission coefficient is presented in Fig. 11 and an analysis of the results indicates the presence of two time scales: a rapid decay with duration of less than 1 ps and a slower time scale on the order of 5–10 ps arising from diffusive barrier crossing dynamics. A plateau is not established on the 10 ps time scale, but there is an exponen-

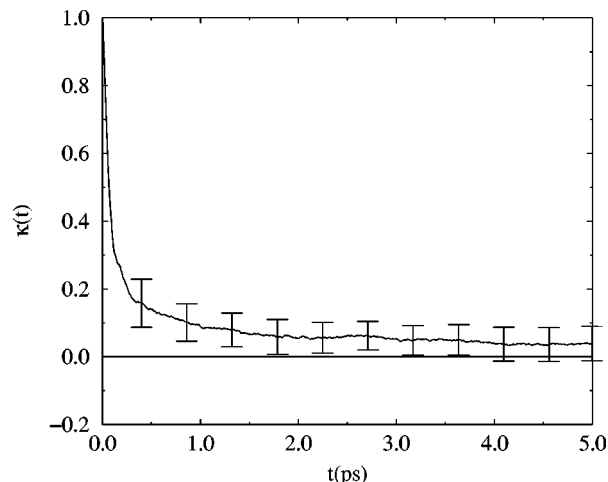


FIG. 11. Transmission coefficient $\kappa(t)$ vs time.

tial decay with a decay constant of 0.21 ps^{-1} . This signals the breakdown of a description in terms of a simple phenomenological first-order rate law for the dynamics of the interconversion process. The relaxation times of other processes that are coupled to the reaction coordinate, such as motion of the solvent particles and shape fluctuations of the cluster, are comparable to that of the flux autocorrelation function of the reaction coordinate.

Diffusive barrier crossing gives rise to a very small value of the transmission coefficient. A detailed examination of the ensemble indicated that a substantial number of trajectories recrossed the transition state one or more times. These factors preclude an accurate estimate of the transmission coefficient. Diffusive barrier crossing is also found in simulations of the dissociation of salt ion pairs in polar solvents in the bulk phase¹¹ but in this case the time scales are such that a plateau is well established.

The origin of the diffusive motion of the reaction coordinate in the cluster is different from that of the bulk phase. In the bulk phase the diffusive barrier crossing arises because of the strong coupling between the solvent and the reaction coordinate. In the cluster environment the fact that the reaction occurs on the surface of the cluster affects the dynamics. Therefore there are trajectories where the coupling of the solvent and the reaction coordinate is very strong and trajectories where the complex is at regions of the surface where the density of the solvent is very low which leads to very low coupling.

In a large number of trajectories the changes in the coordination number of Na^+ do not follow the motion of the reaction coordinate. The reaction occurs in a region of the cluster with large mass density gradients of the solvent. The Cl^- ions are exposed to lower solvent densities than the Na^+ ion, therefore it is mainly the motions of the solvent molecules around Na^+ that determine the dynamics. The water molecules around Na^+ are tightly bound to the ion, and although there are changes in their number and configurations, the times for these changes are long. The low density of solvent surrounding the Na^+Cl^- pairs allows the reaction coordinate to change faster than the reorganization of the

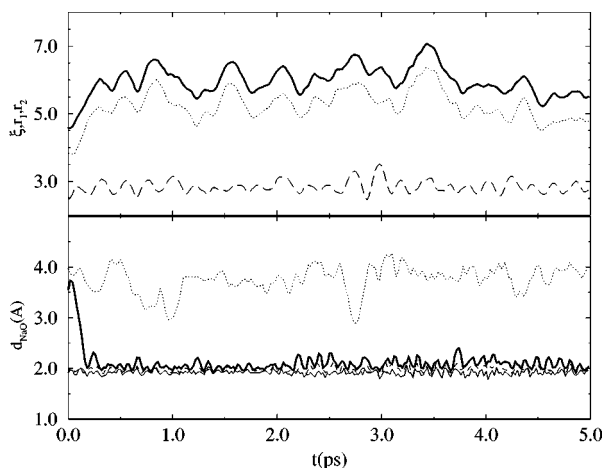


FIG. 12. Upper panel: ξ , solid line, r_1 , dashed line, and r_2 , dotted line, vs. time. Lower panel: the NaO distances of the four closest oxygen sites to Na^+ .

solvent particles. We observe that in a number of trajectories of 5 ps duration the reaction coordinate ξ moves clearly to the product state by the extension of one of the Na^+Cl^- distances and returns again to the reactant state.

Sample trajectories which start at the ξ barrier top and show the behavior discussed above are shown in Figs. 12 and 13. In the first panel of Fig. 12, which shows ξ , r_1 , and r_2 as a function of time, the transition state value of ξ corresponds to r_1/r_2 at the minimum of $W(\phi)$. The lower panel shows the distances of the four closest oxygen sites of water molecules to Na^+ . When r_2 is extended, one water molecule whose dipole moment forms an angle close to 15 deg with \mathbf{r}_{NaO} approaches Na^+ . This trajectory shows a strong coupling between the reaction coordinate and the solvent degrees of freedom that are associated with the first solvation shell of Na^+ . In this case the changes in the number of strongly solvated water molecules tracks the changes in the reaction coordinate.

Figure 13 shows another trajectory where ξ initially has positive velocity directed towards the product state. As is shown clearly in the lower panel the transition state resembles the reactants since two water molecules are tightly

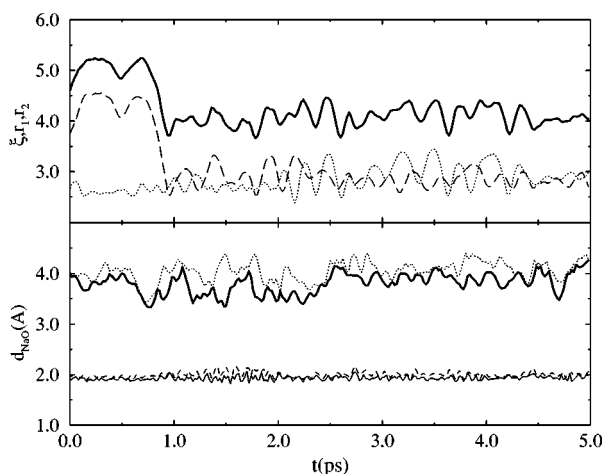


FIG. 13. Same as Fig. 12.

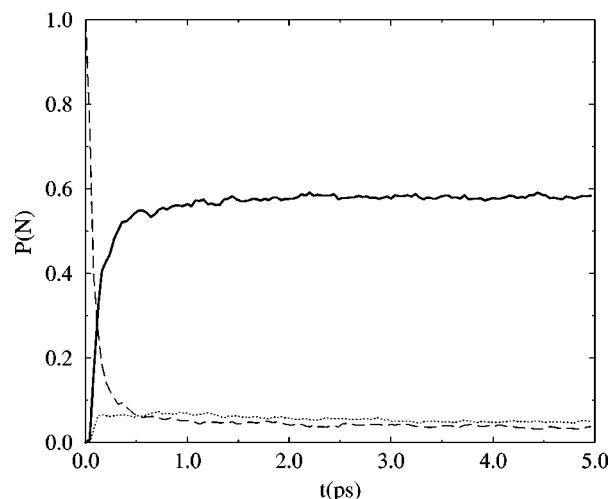


FIG. 14. Probability $P(N)$ vs. time of finding a trajectory in the following regions: (a) $3.8 < \xi < 4.2$, solid line, (b) $4.4 < \xi < 4.75$, dashed line, (c) $5.2 < \xi < 5.6$, dotted line.

bound to Na^+ . The reaction coordinate as well as r_2 show extensive recrossings in 1 ps while the position of the third closest water molecule to Na^+ is not correlated with this recrossing dynamics. Consequently, in this case the coupling of the remaining solvent molecules with the complex is weak. Similar trajectories exist where the reaction coordinate moves to the product state in 5 ps while the number of the water molecules in the first solvation shell of Na^+ does not change. Examination of the dynamics shows that the selection of a reaction coordinate for ion dissociation in clusters is more complicated than in the bulk phase. In the bulk phase due to the strong coupling of the solvent with the reacting system one may envisage a reaction coordinate that is related to the solvent degrees of freedom, for example, the number of water molecules in the first solvation shell of the positive ion. A similar reaction coordinate may not be as useful for reactions in clusters.

We also note that many trajectories with coordinates in the product state are directed towards escaping configurations (free ion forms), since there is a very low energy barrier between the SSIP forms and the free ions.

The distribution of trajectories in various ξ regions vs. time is shown in Fig. 14. Three regions of $\xi(t)$ were monitored that correspond to the reactant, product and transition state. The majority of the trajectories return to the reactant state, since the transition state resembles the reactant state. The fraction of trajectories that end in the product state is similar to the fraction of trajectories that recross the transition state in times greater than the short transient period.

V. CONCLUSIONS

The dissociation dynamics of the $[\text{Na}^+(\text{Cl}^-)_2]$ complex in mesoscopic water clusters was found to proceed in two steps that lead to the formation of single and double solvent-separated configurations. The presence of a second Cl^- affects the reaction mechanism and the two steps of the reaction involve different barrier heights. One might intuitively expect that the dissociation of the first Cl^- would be ener-

getically favorable; however, the dissociation of the complex that leads to the singleSSIP form involves a larger barrier height. This may be considered to be a microscopic version of the salting-out effect. Since the reaction occurs on the surface of the cluster, where the density of the solvent molecules is low, the few water molecules that are available for the solvation of the complex are strongly oriented by the salt complex. When the first dissociation occurs, there is more freedom in the location of the dissociated chloride which allows the solvent to participate more freely in the dissociation of the second chloride ion.

The dynamics of the dissociation process presents interesting features. The barrier crossing is diffusive in character and there are considerable corrections to transition state theory. The decay time of the transmission coefficient is much longer than that observed in simulations in bulk solvents and a plateau is not established in a 10 ps time interval. The shape fluctuations of the cluster and the diffusive motions of the surface solvent molecules contribute to the relaxation processes in the time-dependent transmission coefficient and possible breakdown of simple first-order kinetics. For these reasons mesoscale cluster solvation dynamics is rather different from its bulk counterpart.

¹A. W. Castleman, Jr. and K. H. Bowen, Jr., *J. Phys. Chem.* **100**, 12911 (1996).

²B. J. Greenblatt, M. T. Zanni, and D. M. Newmark, *Science* **276**, 1675 (1997).

³J. F. Garvey, W. J. Herron, and G. Vaidyanathan, *Chem. Rev.* **94**, 1999 (1994).

⁴B. J. Finlayson-Pitts, M. J. Ezell, and J. Pitts, Jr., *Nature (London)* **337**, 241 (1989).

⁵S. Peters and G. Ewing, *J. Phys. Chem.* **100**, 14093 (1996).

⁶S. Winstein, E. Clippinger, A. Fainber, and G. Robinson, *J. Am. Chem. Soc.* **76**, 259 (1954).

⁷H. Sadek and R. Fuoss, *J. Am. Chem. Soc.* **76**, 5897 (1954).

⁸A. Belch, M. Berkowitz, and J. McCammon, *J. Am. Chem. Soc.* **108**, 1755 (1986); O. Karim and J. McCammon, *ibid.* **108**, 1762 (1986); *Chem. Phys. Lett.* **132**, 219 (1986); M. Berkowitz, O. Karim, J. McCammon, and P. Rossky, *ibid.* **105**, 577 (1984).

⁹D. E. Smith and L. X. Dang, *J. Chem. Phys.* **100**, 3757 (1994).

¹⁰E. Guàrdia, R. Rey, and J. Padró, *Chem. Phys. Lett.* **205**, 260 (1993).

¹¹G. Ciccotti, M. Ferrario, J. Hynes, and R. Kapral, *J. Chem. Phys.* **93**, 7137 (1990); *Chem. Phys.* **129**, 241 (1989).

¹²D. Laria and R. Fernández-Prini, *Chem. Phys. Lett.* **205**, 260 (1993); *J. Chem. Phys.* **102**, 7664 (1995).

¹³D. Laria, R. Kapral, D. Estrin, and G. Ciccotti, *J. Chem. Phys.* **104**, 6560 (1996).

¹⁴I. Rips and J. Jortner, *J. Chem. Phys.* **97**, 536 (1992).

¹⁵G. Makov and A. Nitzan, *J. Phys. Chem.* **96**, 2965 (1992).

¹⁶See, for instance, I. Rips and J. Jortner, *J. Chem. Phys.* **97**, 536 (1992); M. Maroncelli and G. R. Fleming, *ibid.* **89**, 5044 (1988).

¹⁷H. J. C. Berendsen, J. R. Grigera, and T. P. Straatsma, *J. Phys. Chem.* **91**, 6269 (1987).

¹⁸J. Alejandre, D. J. Tildesley, and G. A. Chapela, *J. Phys. Chem.* **102**, 4574 (1995).

¹⁹L. Verlet, *Phys. Rev.* **159**, 98 (1967).

²⁰J. Ryckaert, G. Ciccotti, and H. Berendsen, *J. Comput. Phys.* **23**, 327 (1977).

²¹S. Nosé, *Mol. Phys.* **52**, 255 (1984); W. G. Hoover, *Phys. Rev. A* **31**, 1695 (1985).

²²E. Carter, G. Ciccotti, J. Hynes, and R. Kapral, *Chem. Phys. Lett.* **156**, 472 (1989).

²³The “centrifugal” contribution to the free energy, $2 \ln \xi$, arising from the second term in the numerator of Eq. (3), contributes almost 0.5 kT to the energy difference between the first minimum at (2.85, 2.85) and the barrier top, and almost 1.3 kT to the energy difference between the two minima at (2.85, 2.85) and (2.85, 4.7).

²⁴These projections provide clear information on the cluster structure in small size clusters. For large clusters there are many water molecules at the two sides of the plane and their projections on the plane would give a more uniform structure.

²⁵J. Caldwell, L. X. Dang, and P. A. Kollman, *J. Am. Chem. Soc.* **112**, 9145 (1990).

²⁶L. Perera and M. L. Berkowitz, *J. Chem. Phys.* **95**, 1954 (1991).

²⁷T. Yamamoto, *J. Chem. Phys.* **33**, 281 (1960).

²⁸G. Ciccotti and J. P. Ryckaert, *Comput. Phys. Rep.* **4**, 345 (1986).